

## Giant twist-angle dependence of thermal conductivity in bilayer graphene originating from strong interlayer coupling

H. F. Feng, B. Liu , and Zhi-Xin Guo \*

*State Key Laboratory for Mechanical Behavior of Materials, Center for Spintronics and Quantum System, School of Materials Science and Engineering, Xi'an Jiaotong University, Xi'an, Shaanxi 710049, China*



(Received 15 March 2023; revised 7 October 2023; accepted 22 November 2023; published 18 December 2023)

Recently, the twist-angle effect on two-dimensional van der Waals (vdW) materials, such as bilayer graphene, has attracted great attention. Many novel electronic, magnetic, and even optical properties induced by such effects have been discovered. However, the twist-angle effect on a phononic property is not so remarkable. By investigating the thermal conductivity of twisted bilayer graphene (TBG), we reveal that the trivial twist-angle effect on a phononic property observed in previous studies is owing to the nonlocalization nature of phonons. This characteristic makes phonons hardly trapped by the weak interlayer potentials induced by the twist-angle dependent moiré pattern. We propose that the twist-angle effect can be effectively enhanced by increasing the interface coupling. Using a sandwich structure composed of hexagonal boron nitride and TBG, we demonstrate that the thermal conductivity of TBG can be either significantly increased or dramatically decreased under the synergistic modulation of interlayer-coupling strength and twist angle. Particularly, the twist-angle effect can lead to a nontrivial reduction of thermal conductivity by up to 78% when a strong interlayer coupling is applied. The reduction is several times larger than that observed in the freestanding TBG originating from the twist-angle dependent phonon scatterings induced by the edge phonons. The underlying mechanism for the giant twist-angle dependent thermal conductivity is further revealed based on phonon transport theory. Our findings provide a platform for achieving efficient twist-angle modulation on the phonon transport property of vdW materials.

DOI: [10.1103/PhysRevB.108.L241405](https://doi.org/10.1103/PhysRevB.108.L241405)

During the past decade, twisted two-dimensional (2D) materials have attracted extensive attention in both academic research and engineering applications because of their unique and adjustable physical and chemical properties [1–9]. Different from the strong chemical bonding interactions in the in-plane direction, the weak van der Waals (vdW) interactions in the cross-plane direction of 2D materials make it possible to stack and assemble the vdW homogeneous/heterogeneous systems layer by layer, which provides a powerful means for designing and manufacturing 2D stacked materials with intriguing properties [10,11].

In stacked vdW materials, the interlayer twist angle (denoted as  $\psi$ ) has been of special concern in recent years, where the twisted bilayer graphene (TBG) has been the most widely investigated material in both experimental and theoretical studies [12–15]. Specifically, a flat electronic band with vanishing Fermi velocity appears at Dirac points when  $\psi$  becomes particularly small (a so-called magic angle) [16]. As a result, the relatively strong coupling between interlayer electrons around the moiré point gives rise to certain filling states of the flat band and thus a series of novel properties on electrons [17,18], magnets [19–22], photons [23–25], etc. For instance, metal-insulator transition and superconducting states appear with  $\psi = 1.1^\circ$  and  $1.05^\circ$ , respectively [18,26,27]. Emergent superstable ferromagnetism was discovered with  $\psi = 1.2^\circ$  [19]. In addition, the moiré patterns of TBG become

a natural plasmon photonic crystal for propagating nanolight with  $\psi = 0.06^\circ$  [28].

On the other hand, the twist-angle effect of a phononic property is not so attractive [29]. Although extensive theoretical and experimental investigations have been carried out under various conditions, the twist-angle effect only leads to a maximum reduction of thermal conductivity ( $\kappa$ ) in TBG by about 30% [30–33]. Such variation of  $\kappa$  is trivial in comparison with the result of edge effect, defect effect, etc. [34–37]. Moreover,  $\kappa$  does not obviously depend on the twist angle but has a V-shaped relationship with the commensurate lattice constant where the lowest  $\kappa$  appears around 1 nm [31]. Note that the electronic thermal conductivity is usually much smaller than the phononic one in graphene [38,39], thus the role of electrons in thermal conductivity of TBG is expected to be insignificant. Hence, why the twist-angle effect of a phononic property is so inferior to that of the electronic ones is still to be clarified. Moreover, from both fundamental research and practical application points of view, there is a great need to find an efficient way to enhance the twist-angle effect on the phonon transport property effectively.

By investigating the  $\kappa$  of TBG based on the molecular dynamics simulations and phonon transport theory, we reveal the intrinsic mechanism for the weak twist-angle effect on the phonon transport property. We find that the trivial twist-angle effect on the thermal conductivity of TBG is owing to the nature of the nonlocalization of phonons, which makes phonons hardly trapped by the weak vdW interlayer potentials induced by the moiré pattern. We also find that the twist-angle

\*zxguo08@xjtu.edu.cn

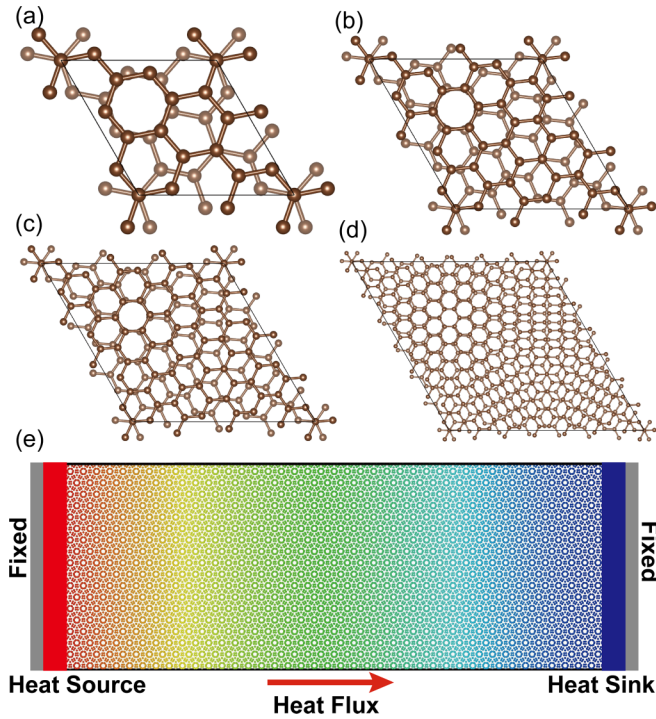


FIG. 1. Top views of the primitive cells of TBGs with various twist angles ( $\psi$ ). (a)  $\psi = 21.79^\circ$ ; (b)  $\psi = 13.17^\circ$ ; (c)  $\psi = 9.43^\circ$ ; (d)  $\psi = 5.09^\circ$  TBG. (e) NEMD model with simplified scales of in-plane conduction. The gray region corresponds to the fixed layers, the red region denotes the heat source, the blue region represents the heat sink, and the colored region indicates the region of heat transfer.

effect can be effectively enhanced by increasing the interlayer coupling, demonstrated in a sandwich structure composed of hexagonal boron nitride (h-BN) and TBG.

To verify the twist-angle effect on thermal conductivity, we first consider a TBG 90 nm in length (i.e., 90 nm  $\times$  10 nm in the  $x$ - $y$  plane with heat flux in the  $x$  direction) and adopt a periodic boundary condition in the width ( $y$ ) direction (denoted as 2D TBG). Here we mainly consider the TBGs with  $\psi = 21.79^\circ$ ,  $13.17^\circ$ ,  $9.43^\circ$ , and  $5.09^\circ$ , respectively [Figs. 1(a)–1(d)], which present distinguishable moiré patterns [40]. To explore the magic angle effect on thermal conductivity, we have additionally considered the TBG with  $\psi = 1.08^\circ$ . As indicated in Fig. 1(e), the nonequilibrium molecular dynamics (NEMD) method is used to obtain the thermal conductivity (see Sec. SI in the Supplemental Material [41]). According to our simulations, the 10 nm width is large enough to get a converged thermal conductivity in the periodic boundary condition. Figure 2(a) shows the twist-angle dependent thermal conductivity of TBG with different temperatures. It is found that the thermal conductivity hardly changes with a twist angle at room temperature (300 K). Although the twist-angle effect becomes more significant at the low-temperature region (50 K), the variation of thermal conductivity difference is still very small, which is within 9.6% (from 3540 to 3200 W/mK, and from 1352 to 1223 W/mK after quantum corrections; see Sec. SII in the Supplemental Material [41]). Such a weak twist-angle effect on thermal conductivity, which is negligible in comparison with the experimental observations (20%–30% variation at room temperature [31,32]), is unexpected.

It is noted that the periodic boundary condition in the width direction is adopted in our NEMD simulations, where the phonon scatterings induced by the edge phonons in the width direction are eliminated. Whereas, in the experiments, the TBG always has edge phonons due to its finite width. This may be the reason for the much weaker twist-angle effect on thermal conductivity in our results. To verify such

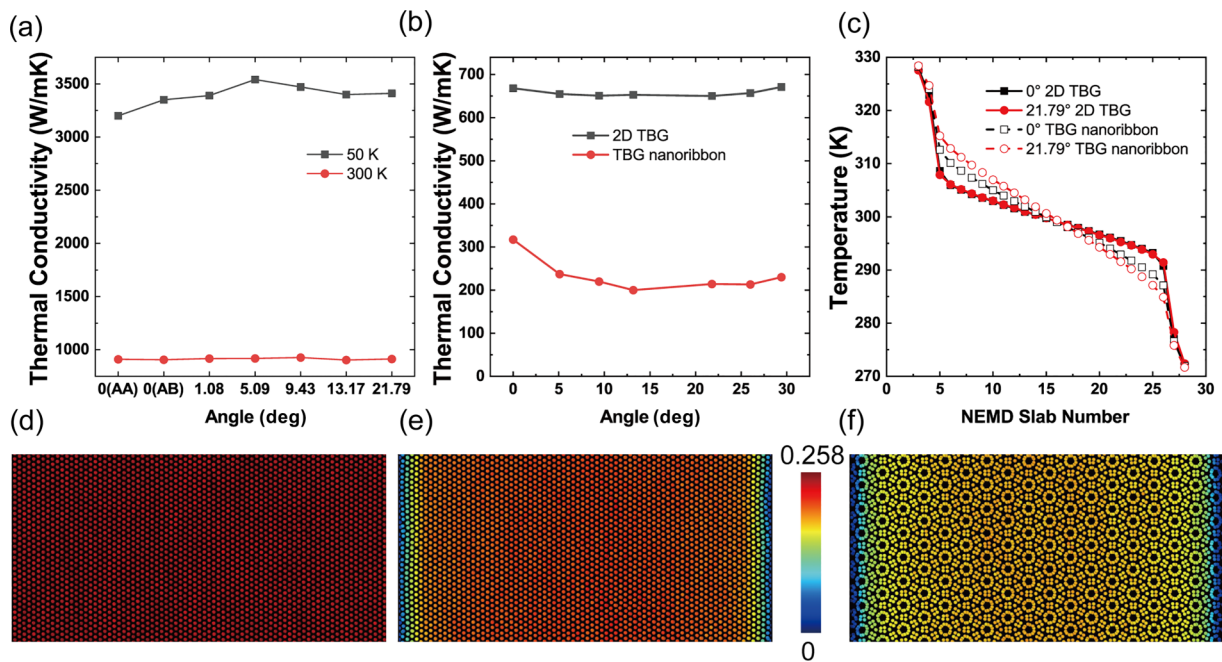


FIG. 2. (a) Thermal conductivity of 2D TBG as a function of twist angle at different temperatures (90 nm  $\times$  10 nm). (b) Thermal conductivity of TBG and TBG nanoribbons as a function of twist angle (30 nm  $\times$  10 nm). (c) Temperature profile as a function of NEMD slab index for 2D TBG and TBG nanoribbons. Spatial distribution of heat flux accumulation of (d)  $\psi = 0^\circ$  for 2D TBG, (e)  $\psi = 0^\circ$  for TBG nanoribbon, and (f)  $\psi = 21.79^\circ$  for TBG nanoribbon.

speculation, we further calculate the thermal conductivity of TBG nanoribbons ( $30 \text{ nm} \times 10 \text{ nm}$  in the  $x$ - $y$  plane), where the armchair edge is considered as zero angle, and the shrink-wrapped boundary condition is applied in the width direction. As shown in Fig. 2(b), thermal conductivity first decreases and then increases with the twist angle increasing, reaching the minimum value ( $200 \text{ W/mK}$ ) at  $13.17^\circ$ , which is 37% lower than that at  $0^\circ$  ( $317 \text{ W/mK}$ ). This result is different from that obtained in 2D TBG but agrees well with the experimental observations and other theoretical calculations [30–33].

Figure 2(c) additionally shows the temperature distributions in the length direction of the simulated TBGs. A common feature is that TBG nanoribbons have obviously larger temperature gradients than 2D TBGs. Moreover, the temperature gradient in 2D TBGs is nearly independent of the twist angle, opposite to that in TBG nanoribbons. In Figs. 2(d)–2(f) we additionally show the heat flux distributions in 2D TBG and TBG nanoribbons. Different from the 2D TBG with a uniform large heat flux distribution [Fig. 2(d)], there are remarkable nonuniform and twist-angle dependent heat flux distributions in TBG nanoribbons. As shown in Figs. 2(e) and 2(f), the heat flux becomes particularly small around the edges of nanoribbons, showing the nature of strong boundary scatterings induced by the edge phonons, which leads to the reduction of heat flux. Notably, the heat flux of a TBG nanoribbon with  $\psi = 21.79^\circ$  is much smaller than that of  $\psi = 0^\circ$ , which is distinct even in the center region, showing that the edge phonons can lead to a significant reduction of heat flux in the whole TBG region. The underlying mechanism can be attributed to the strong scatterings between edge phonons and body phonons, the extent of which depends on the specific edge structures determined by twist angle. This is because the different edge chirality corresponds to distinct edge phonons and thus the distinct scatterings. Such argument is confirmed by the calculated frequency dependent thermal conductivity of 2D TBG and TBG nanoribbons shown in Supplemental Material Fig. S2. Therefore, the 20%–30% variation of thermal conductivity reported in previous studies is, in fact, due to the edge phonons, which have a localized characteristic (see Sec. SIII in the Supplemental Material [41] for details).

The above results, on the other hand, show that the vdW interlayer potential induced by the moiré pattern is too weak to trap phonons, which results in little change of thermal conductivity. This is because phonons are collectively excited quasiparticles in nature, which are hardly localized in a defect-free system. Hence, the weak twist-angle effect is not expected for other particles (such as electrons, magnets, and photons), whose singularity strongly correlates to the localized electrons near the moiré points [16,64]. This feature also explains the absence of a flat band in the phonon dispersions with a magic angle ( $1.05^\circ$ ) [65] that had been widely observed in the electronic systems [18].

Accordingly, exotic twist-angle effect on the thermal conductivity of TBG can be expected when the interlayer interaction is effectively enhanced. It is known that an easy way to enhance interlayer interaction is by reducing the interlayer distance ( $d_{\text{int}}$ ) by pressurizing. Hence, we construct a h-BN/TBG/h-BN sandwich structure, where  $d_{\text{int}}$  can be

effectively reduced by decreasing the distance between the h-BN layers under and above the TBG. As shown in Figs. 3(a) and 3(b), two sandwich structures are considered: (1) h-BN layers synchronously rotate with their adjacent graphene layers (denoted as Cor structure), so that the rotation angle between the h-BN layer and its adjacent graphene is always  $0^\circ$  as shown in Fig. 3(c); (2) h-BN layers remain unrotated during the rotation of graphene layers (denoted as Uncor structure). In the Uncor structure, additional moiré patterns between h-BN and its adjacent graphene layers would be formed due to the nonzero twist angle [Fig. 3(d)]. Moreover, in order to clearly exhibit the interlayer interaction effect on the thermal conductivity of TBG, the vibration of h-BN layers is frozen during the simulation. Note that a  $30 \text{ nm} \times 10 \text{ nm}$  sandwich structure is considered in the simulation, where the periodic boundary condition is applied in the width direction to eliminate the influence of edge phonons.

Figure 4(a) shows the calculated twist-angle dependent thermal conductivity of TBG in both Cor and Uncor structures at 300 K. In order to make a direct contradistinction, the thermal conductivity of freestanding TBG is also shown in Fig. 4(a), which exhibits a slight variation with the twist angle due to perturbation of the simulated TBG length. A common feature is that the twist-angle dependence of thermal conductivity in both Cor and Uncor structures is very similar to that in the freestanding TBG when the interlayer interaction is weak ( $d_{\text{int}} = 3.4$  and  $3.1 \text{ \AA}$ ). This feature can be owing to the analogous phonon band structures of TBG in Cor and Uncor structures, as illustrated in Supplemental Material Fig. S5(a). This result also agrees with our expectation that the weak interlayer interaction cannot lead to a significant twist-angle effect on thermal conductivity, even with the additional interface interaction from h-BN. Nevertheless, an interesting phenomenon is observed, i.e., thermal conductivity of TBG is obviously increased in the sandwich structures. To eliminate the influence from perturbation of the simulated TBG length, we further calculate the change ratio of thermal conductivity, which is defined as

$$\Delta\kappa = \frac{\kappa_1 - \kappa_0}{\kappa_0} \times 100\%, \quad (1)$$

where  $\kappa_0$  and  $\kappa_1$  are the twist-angle dependent thermal conductivity of TBG in the freestanding and sandwich structures, respectively. As shown in Fig. 4(b), on the one hand,  $\Delta\kappa$  has little twist-angle dependence in the sandwich structures. On the other hand,  $\Delta\kappa$  obviously increases with the reduction of  $d_{\text{int}}$  from 3.4 to 3.1  $\text{\AA}$ , where a sizable increment of about 10% can be obtained with  $d_{\text{int}} = 3.1 \text{ \AA}$  in both Cor and Uncor structures. The unusual increase of thermal conductivity is mostly attributed to the interlayer interaction from h-BN, which lifts the out-of-plane ZA1 and ZA2 phonon branches in TBG [66,67] (note that the LA and TA modes exhibit a much smaller change with  $d_{\text{int}}$ ), and thus leads to the reduction of phonon-phonon scatterings (see Sec. SIV in the Supplemental Material [41]).

When the interlayer distance is further reduced to  $d_{\text{int}} = 2.8 \text{ \AA}$  (interlayer interaction becomes 4.4 times larger than that of  $d_{\text{int}} = 3.1 \text{ \AA}$ ), the variation of  $\kappa$  becomes dramatic. As shown in Fig. 4(a), the thermal conductivity of  $\psi = 0^\circ$  (AB stacking) is significantly larger than that of  $\psi > 0^\circ$  in both

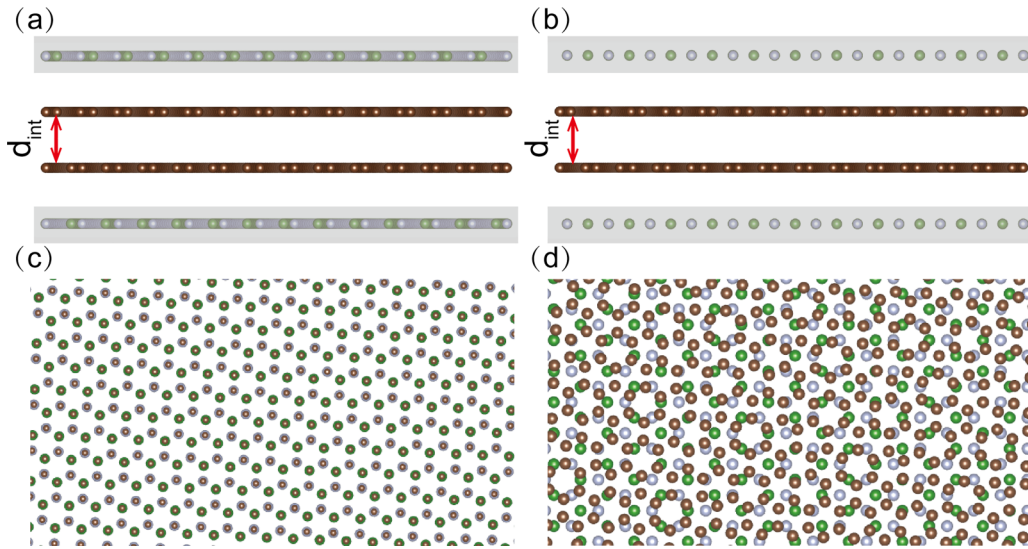


FIG. 3. Schematic structures of TBG sandwiched between two fixed h-BN layers of both Cor and Uncor structures. (a) Top view of Cor structure. (b) Top view of Uncor structure. (c) Side view of Cor structure. (d) Side view of Uncor structure.  $d_{\text{int}}$  represents the interlayer distance between two graphene layers. The green, saddle brown, and gray balls represent the B, C, and N atoms, respectively. The fixed h-BN layers are indicated by the semitransparent rectangle.

Cor and Uncor structures. Note that the thermal conductivity of the Cor and Uncor structures presents contrary behavior under the strong interface coupling: it is increased in the Cor structure but significantly decreased in the Uncor structure. This result can be understood from the distinct phonon dispersions due to the different interfacial interactions from h-BN (see Sec. SVI in the Supplemental Material [41]). On the one hand, the interaction from h-BN leads to a significant divergence of phonon band structures between the Cor and Uncor structures for the ZA modes, and thus the distinct thermal conductivities [Fig. S5(b)]. On the other hand, the h-BN layers in the Cor (Uncor) structure can be recognized as a smooth (rough) surface for the phonon propagation in TBG, which makes the TBGs in the Uncor structure have smaller thermal

conductivity. It is noticed that the maximum thermal conductivity appears in the Cor structure (852 W/mK) with  $\psi = 0^\circ$ , which is about 27% larger than that of freestanding TBG (672 W/mK). This result shows that proper interface coupling can be an efficient way to increase the thermal conductivity of a bilayer system, which has great potential applications in heat management in chips. As shown in Fig. 4(b), in both Cor and Uncor structures  $\Delta\kappa$  remarkably decreases by about 20% with  $\psi$  increasing from  $0^\circ$  to  $5.09^\circ$ , and then slightly increases by about 5% with  $\psi$  increasing from  $5.09^\circ$  to  $21.79^\circ$ . This result verifies that the increase of interlayer interaction to a certain extent can effectively enhance the twist-angle effect on phonon transport properties due to the significant modulation of phonon band structures and thus phonon-phonon scatterings induced by the moiré-pattern potential (see Sec. SV in the Supplemental Material [41]). Note that the strong interlayer interaction in this context results in not only a lift of the ZA branches but also an upward shift and splitting of the LA and TA branches, which increases the phonon scatterings at low-frequency regions and thus a reduction of thermal conductivity at certain twist angles (see Sec. SIV in the Supplemental Material [41]).

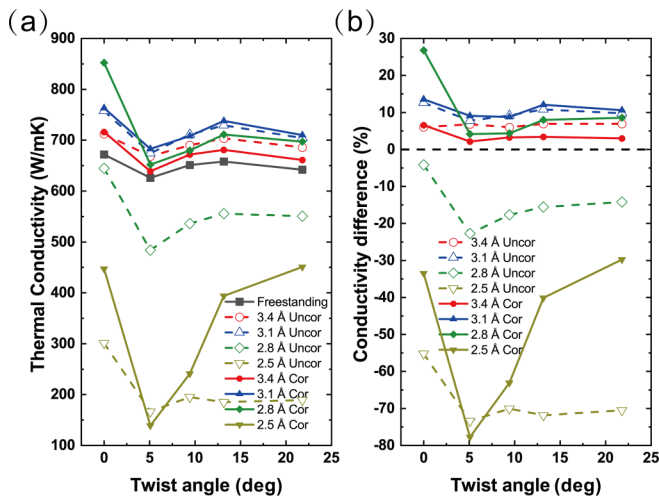


FIG. 4. (a) Thermal conductivity and (b) conductivity difference of 2D TBGs in Cor and Uncor structures with various interlayer distances as a function of twist angle.

More exotic variations of thermal conductivity can be obtained when the interlayer interaction is further increased. As shown in Fig. 4(a), with  $d_{\text{int}}$  decreased to 2.5 Å (interlayer interaction becomes 17.2 times larger than that of  $d_{\text{int}} = 3.1$  Å), the thermal conductivity in both Cor and Uncor structures is extraordinarily smaller than the freestanding one. The underlying mechanism can be generally understood from the competing effect from the significant upshift of the out-of-plane ZA1/ZA2 and in-plane LA2/TA2 branches [66,67], where the negative effect from the upshift of the LA2 and TA2 branches becomes dominating (as shown in Fig. S3(e)), all four low-frequency phonon branches show significant upshift and strong crossing/splitting, resulting in severe scattering and thus a significant decrease in thermal conductivity

contribution. Also, see Sec. SIV in the Supplemental Material [41]). Notably, the maximum thermal conductivity in the Cor and Uncor structures is 447 and 301 W/mK, respectively; 33% and 55% smaller than that of freestanding TBG. Note that the maximum thermal conductivity in the Cor structure appears with  $\psi = 21.79^\circ$ . This is different from the cases with weaker interlayer interaction as well as that in the Uncor structure, where the maximum thermal conductivity exists with  $\psi = 0^\circ$ . Meanwhile, the minimum thermal conductivity in both Cor (139 W/mK) and Uncor (167 W/mK) structures appears with  $\psi = 5.09^\circ$ , where  $\Delta\kappa$  reaches up to 78% and 73%, respectively. This result shows that a giant reduction of thermal conductivity in vdW materials can be easily realized under the synergistic effect of strong interlayer interaction and nonzero twist angle, which may have potential applications in thermal insulations and thermoelectrics.

In addition, distinguished twist-angle dependent thermal conductivity can be induced by strong interlayer interactions in both Cor and Uncor structures. In order to explore the maximum variation of thermal conductivity induced by the twist-angle effect, we further explore the maximum difference of  $\Delta\kappa$  which is defined as

$$\gamma = \frac{\kappa_{\max} - \kappa_{\min}}{\kappa_{\max}} \times 100\%, \quad (2)$$

where  $\kappa_{\max}$  and  $\kappa_{\min}$  are the maximum and minimum thermal conductivity of TBG with various twist angles but the same  $d_{\text{int}}$ , respectively. It is found that  $\gamma$  in the Cor and Uncor structures reaches up to 69% and 45%, respectively; much more significant than that originated from edge effects in TBG nanoribbons. This simulation result also agrees well with our proposed mechanism, that is, the strong interlayer interaction can remarkably enhance the effect of moiré-pattern potential on phonons. Note that the twist-angle effect in the Cor structure is much more profound than that in the Uncor structure, especially in the nonzero twist-angle region. This is because there is an additional twist-angle (or moiré pattern) effect in the Uncor structure, originating from the relative rotation between graphene and its nearby h-BN layers (as indicated in Fig. 3). The “double” moiré patterns make thermal conductivity in TBG easily saturated to a certain value and thus robust to nonzero twist angles under the strong interlayer interactions. Thus, the extensive modulation of thermal conductivity can be realized under the synergistic effect of strong interlayer interaction and nonzero twist angle.

Finally, we reveal the mechanism for the unusually large reduction of thermal conductivity at a small twist angle ( $5.09^\circ$ ) under the strong interlayer interaction in the Cor structure. We first show in Fig. 5(a) the temperature distribution in the Cor structures with  $\psi = 5.09^\circ$  and  $21.79^\circ$ , corresponding to the smallest and largest thermal conductivity, respectively. It is found that there is a large temperature jump in the  $5.09^\circ$  structure, while it is absent in the  $21.79^\circ$  structure. A temperature jump usually means the existence of a thermal interface that hinders phonon transport. To unveil the reason for such an interesting phenomenon, we further extract the atomic structures during the NEMD simulation at 300 K. As shown in Fig. 5(b), there is indeed an additional small moiré pattern appearing in the middle of the TBG in the  $5.09^\circ$  structure (here we call it “moiré junction” [69]). Such

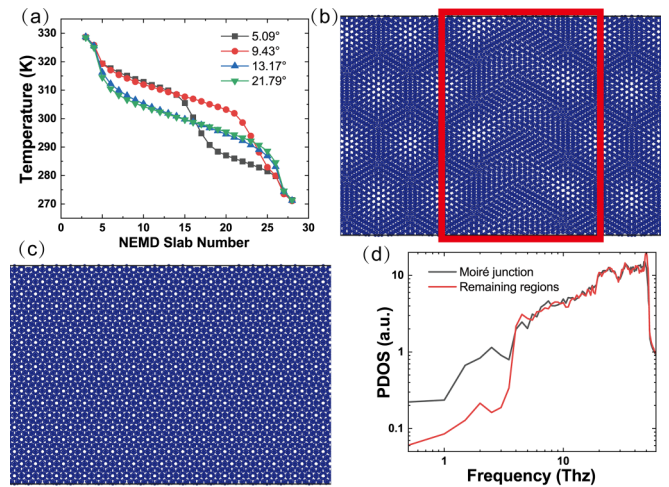


FIG. 5. (a) Temperature profiles as a function of NEMD slab index for 2D TBGs in Cor structure with various twist angles at  $d_{\text{int}} = 2.5 \text{ \AA}$ . (b) and (c) Schematic structures of TBGs in Cor structure ( $d_{\text{int}} = 2.5 \text{ \AA}$ ) with  $\psi = 5.09^\circ$  and  $\psi = 21.79^\circ$ , respectively. The moiré junction in (b) is indicated by the red quadrangle. (d) PDOS of the moiré junction and the normal region of the TBG structure are shown in (b).

a new moiré pattern transforms the simulated TBG into a homojunction structure. As shown in Fig. 5(c), the moiré junction is absent in the large twist-angle ( $21.79^\circ$ ) structure, so the temperature distribution becomes very smooth in the thermal conduction region. Figure 5(d) additionally shows the phonon density of states (PDOS) in the moiré junction, compared with that in the remaining regions, as marked in Fig. 5(b). It is seen that a significant mismatch exists between the two PDOS in the low-energy region (below 3.5 THz), indicating the distinct phonon band structures in the two TBG regions. Consequently, the low-energy phonons will receive additional scatterings when propagating across the moiré junction, which leads to the thermal interface and thus the reduction of thermal conductivity [70].

Before concluding, it should be pointed out that the h-BN/TBG/h-BN sandwich structures considered in the simulation are based on a simplified model where the vibration of h-BN layers is artificially frozen. Nevertheless, the obtained physics is still valid in real systems. For example, we have additionally considered the multilayer h-BN/TBG/multilayer h-BN structure where the h-BN layers nearby TBG can freely vibrate [Figs. S6(a) and 3(b)]. As shown in Figs. S6(c) and S6(d), the obtained twist-angle and interlayer-distance dependence of thermal conductivity is very similar to that in the simplified model. This feature can be owing to the fact that the vibration of h-BN does not significantly affect the phonon band structures of TBG (see Fig. S7). In addition, we have explored the twist-angle effect on the thermal conductivity of TBGs with different simulation lengths and interlayer interaction potential (Kolmogorov-Crespi potential [71]), and similar results are obtained (see Secs. SVII and SVIII in the Supplemental Material [41]). It is also noticed that recently the twist-angle dependent thermal conductivity of TBGs has also been explored based on the homogeneous nonequilibrium molecular dynamics (HNEMD) simulations, where a

local minimum thermal conductivity at  $\psi = 1.08^\circ$  was obtained [72]. While, the distinct simulated sizes for different twist angles [72] may also contribute to the twist-angle dependent thermal conductivity in the HNEMD simulations.

In summary, we have explored intrinsic mechanisms for the twist-angle effect on phonon transport properties. Based on the NEMD simulations for both TBG nanoribbons and 2D TBG, we clarify that the trivial twist-angle effect on the phononic property of 2D TBG is owing to the nature of the nonlocalization of phonons. It makes phonons hardly trapped by the moiré-pattern resulting from interlayer potentials. The slight twist-angle dependent thermal conductivity of TBG observed in experiments, in fact, originates from the phonon scatterings induced by the edge phonons. We additionally propose that the twist-angle effect on phonons can be effectively enhanced by increasing the interface coupling, which can be realized in the h-BN/TBG/h-BN sandwich structures. The thermal conductivity of TBG can be either obviously

increased or remarkably decreased under the synergistic effect of interlayer-coupling strength and twist angle. Notably, the twist-angle effect can lead to a reduction of thermal conductivity several times larger than that induced by the edge phonons in the freestanding TBG nanoribbons. The underlying mechanism for these results is further explained based on the phonon transport theory. Finally, we would like to remark that the giant twist-angle dependence of thermal conductivity induced by strong interface interactions should be generally applied to other twisted vdW materials, such as bilayer transition metal dichalcogenides and buckled graphenelike structures.

We thank Xin-Gao Gong for valuable discussions. We acknowledge financial support from the Ministry of Science and Technology of the People's Republic of China (Grant No. 501100002855) and the Natural Science Foundation of China (Grant No. 12074301).

- 
- [1] G. Abbas, Y. Li, H. Wang, W. X. Zhang, C. Wang, and H. Zhang, Recent advances in twisted structures of flatland materials and crafting moiré superlattices, *Adv. Funct. Mater.* **30**, 2000878 (2020).
- [2] Y. Chu, F. Zhu, L. Wen, W. Chen, Q. Chen, and T. Ma, Superconductivity in twisted multilayer graphene: A smoking gun in recent condensed matter physics, *Chin. Phys. B* **29**, 117401 (2020).
- [3] Z. Gao, M. Q. Zhao, M. M. Alam Ashik, and A. T. C. Johnson, Recent advances in the properties and synthesis of bilayer graphene and transition metal dichalcogenides, *J. Phys.: Mater.* **3**, 042003 (2020).
- [4] Z. Sun and Y. H. Hu, How magical is magic-angle graphene? *Matter* **2**, 1106 (2020).
- [5] K. Tang and W. Qi, Moiré-pattern-tuned electronic structures of van der Waals heterostructures, *Adv. Funct. Mater.* **30**, 2002672 (2020).
- [6] L. Du, T. Hasan, A. Castellanos-Gomez, G. B. Liu, Y. Yao, C. N. Lau, and Z. Sun, Engineering symmetry breaking in 2D layered materials, *Nat. Rev. Phys.* **3**, 193 (2021).
- [7] Y. D. Liao, X. Y. Xu, Z. Y. Meng, and J. Kang, Correlated insulating phases in the twisted bilayer graphene, *Chin. Phys. B* **30**, 017305 (2021).
- [8] D. Huang, J. Choi, C. K. Shih, and X. Li, Excitons in semiconductor moiré superlattices, *Nat. Nanotechnol.* **17**, 227 (2022).
- [9] C. N. Lau, M. W. Bockrath, K. F. Mak, and F. Zhang, Reproducibility in the fabrication and physics of moiré materials, *Nature (London)* **602**, 41 (2022).
- [10] K. Zhang and E. B. Tadmor, Energy and moiré patterns in 2D bilayers in translation and rotation: A study using an efficient discrete-continuum interlayer potential, *Extreme Mech. Lett.* **14**, 16 (2017).
- [11] E. Burzuri, M. Vera-Hidalgo, E. Giovanelli, J. Villalva, A. Castellanos-Gomez, and E. M. Perez, Simultaneous assembly of van der Waals heterostructures into multiple nanodevices, *Nanoscale* **10**, 7966 (2018).
- [12] Y. Chu, L. Liu, Y. Yuan, C. Shen, R. Yang, D. Shi, W. Yang, and G. Zhang, A review of experimental advances in twisted graphene moiré superlattice, *Chin. Phys. B* **29**, 128104 (2020).
- [13] A. Nimbalkar and H. Kim, Opportunities and challenges in twisted bilayer graphene: A review, *Nano-Micro Lett.* **12**, 126 (2020).
- [14] F. He, Y. Zhou, Z. Ye, S. H. Cho, J. Jeong, X. Meng, and Y. Wang, Moiré patterns in 2D materials: A review, *ACS Nano* **15**, 5944 (2021).
- [15] E. Y. Andrei and A. H. MacDonald, Graphene bilayers with a twist, *Nat. Mater.* **19**, 1265 (2020).
- [16] R. Bistritzer and A. H. MacDonald, Moiré bands in twisted double-layer graphene, *Proc. Natl. Acad. Sci. USA* **108**, 12233 (2011).
- [17] M. Yankowitz, S. W. Chen, H. Polshyn, Y. X. Zhang, K. Watanabe, T. Taniguchi, D. Graf, A. F. Young, and C. R. Dean, Tuning superconductivity in twisted bilayer graphene, *Science* **363**, 1059 (2019).
- [18] Y. Cao, V. Fatemi, S. Fang, K. Watanabe, T. Taniguchi, E. Kaxiras, and P. Jarillo-Herrero, Unconventional superconductivity in magic-angle graphene superlattices, *Nature (London)* **556**, 43 (2018).
- [19] A. L. Sharpe, E. J. Fox, A. W. Barnard, J. Finney, K. Watanabe, T. Taniguchi, M. A. Kastner, and D. Goldhaber-Gordon, Emergent ferromagnetism near three-quarters filling in twisted bilayer graphene, *Science* **365**, 605 (2019).
- [20] M. Serlin, C. L. Tschirhart, H. Polshyn, Y. Zhang, J. Zhu, K. Watanabe, T. Taniguchi, L. Balents, and A. F. Young, Intrinsic quantized anomalous Hall effect in a moiré heterostructure, *Science* **367**, 900 (2020).
- [21] C. C. Liu, L. D. Zhang, W. Q. Chen, and F. Yang, Chiral spin density wave and  $d + id$  superconductivity in the magic-angle-twisted bilayer graphene, *Phys. Rev. Lett.* **121**, 217001 (2018).
- [22] M. Xie and A. H. MacDonald, Nature of the correlated insulator states in twisted bilayer graphene, *Phys. Rev. Lett.* **124**, 097601 (2020).
- [23] G. W. Hu, Q. D. Ou, G. Y. Si, Y. J. Wu, J. Wu, Z. G. Dai, A. Krasnok, Y. Mazor, Q. Zhang, Q. L. Bao, C. W. Qiu, and A. Alu, Topological polaritons and photonic magic angles in twisted  $\alpha$ -MoO<sub>3</sub> bilayers, *Nature (London)* **582**, 209 (2020).
- [24] J. Wang, W. Bo, Y. Ding, X. Wang, and X. Mu, Optical, optoelectronic, and photoelectric properties in moiré

- superlattices of twist bilayer graphene, *Mater. Today Phys.* **14**, 100238 (2020).
- [25] J. Wang, X. Mu, L. Wang, and M. Sun, Properties and applications of new superlattice: Twisted bilayer graphene, *Mater. Today Phys.* **9**, 100099 (2019).
- [26] B. Lian, Z. Wang, and B. A. Bernevig, Twisted bilayer graphene: A phonon-driven superconductor, *Phys. Rev. Lett.* **122**, 257002 (2019).
- [27] L. Zou, H. C. Po, A. Vishwanath, and T. Senthil, Band structure of twisted bilayer graphene: Emergent symmetries, commensurate approximants, and Wannier obstructions, *Phys. Rev. B* **98**, 085435 (2018).
- [28] S. S. Sunku, G. X. Ni, B. Y. Jiang, H. Yoo, A. Sternbach, A. S. McLeod, T. Stauber, L. Xiong, T. Taniguchi, K. Watanabe, P. Kim, M. M. Fogler, and D. N. Basov, Photonic crystals for nano-light in moiré graphene superlattices, *Science* **362**, 1153 (2018).
- [29] W. Ren, J. Chen, and G. Zhang, Phonon physics in twisted two-dimensional materials, *Appl. Phys. Lett.* **121**, 140501 (2022).
- [30] X. H. Nie, L. Zhao, S. Deng, Y. Zhang, and Z. Y. Du, How interlayer twist angles affect in-plane and cross-plane thermal conduction of multilayer graphene: A non-equilibrium molecular dynamics study, *Int J. Heat Mass Transfer* **137**, 161 (2019).
- [31] S. Han, X. H. Nie, S. Z. Gu, W. Y. Liu, L. C. Chen, H. Ying, L. Wang, Z. H. Cheng, L. Zhao, and S. S. Chen, Twist-angle-dependent thermal conduction in single-crystalline bilayer graphene, *Appl. Phys. Lett.* **118**, 193104 (2021).
- [32] H. Y. Li, H. Ying, X. P. Chen, D. L. Nika, A. I. Cocemasov, W. W. Cai, A. A. Balandin, and S. S. Chen, Thermal conductivity of twisted bilayer graphene, *Nanoscale* **6**, 13402 (2014).
- [33] C. Li, B. Debnath, X. Tan, S. Su, K. Xu, S. Ge, M. R. Neupane, and R. K. Lake, Commensurate lattice constant dependent thermal conductivity of misoriented bilayer graphene, *Carbon* **138**, 451 (2018).
- [34] Z. X. Guo, D. Zhang, and X. G. Gong, Thermal conductivity of graphene nanoribbons, *Appl. Phys. Lett.* **95**, 163103 (2009).
- [35] J. Hu, X. Ruan, and Y. P. Chen, Thermal conductivity and thermal rectification in graphene nanoribbons: A molecular dynamics study, *Nano Lett.* **9**, 2730 (2009).
- [36] Y. Wang, B. Qiu, and X. Ruan, Edge effect on thermal transport in graphene nanoribbons: A phonon localization mechanism beyond edge roughness scattering, *Appl. Phys. Lett.* **101**, 013101 (2012).
- [37] Y. Y. Zhang, Y. Cheng, Q. X. Pei, C. M. Wang, and Y. Xiang, Thermal conductivity of defective graphene, *Phys. Lett. A* **376**, 3668 (2012).
- [38] T. Y. Kim, C. H. Park, and N. Marzari, The electronic thermal conductivity of graphene, *Nano Lett.* **16**, 2439 (2016).
- [39] M. V. Fischetti and W. G. Vandenberghe, Mermin-Wagner theorem, flexural modes, and degraded carrier mobility in two-dimensional crystals with broken horizontal mirror symmetry, *Phys. Rev. B* **93**, 155413 (2016).
- [40] K. M. M. Habib, S. S. Sylvia, S. Ge, M. Neupane, and R. K. Lake, The coherent interlayer resistance of a single, rotated interface between two stacks of AB graphite, *Appl. Phys. Lett.* **103**, 243114 (2013).
- [41] See Supplemental Material at <http://link.aps.org/supplemental/10.1103/PhysRevB.108.L241405> for the computational method; quantum corrections to the thermal conductivity of TBG; mechanism of edge scattering affecting thermal conductivity; mechanism for the interlayer-distance dependent thermal conductivity; mechanism for the enhanced twist-angle effect on thermal conductivity; mechanism for the difference of thermal conductivity between Cor and Uncor structures; twist-angle dependent thermal conductivity of TBGs with various TBG lengths; and twist-angle dependent thermal conductivity of TBGs with Kolmogorov-Crespi potential for the interlayer interaction. It also contains Refs. [42–63].
- [42] S. Plimpton, Fast parallel algorithms for short-range molecular dynamics, *J. Comput. Phys.* **117**, 1 (1995).
- [43] A. Stukowski, Visualization and analysis of atomistic simulation data with OVITO—the Open Visualization Tool, *Modell. Simul. Mater. Sci. Eng.* **18**, 015012 (2010).
- [44] L. Lindsay and D. A. Broido, Optimized Tersoff and Brenner empirical potential parameters for lattice dynamics and phonon thermal transport in carbon nanotubes and graphene, *Phys. Rev. B* **81**, 205441 (2010).
- [45] C. Si, X. D. Wang, Z. Fan, Z. H. Feng, and B. Y. Cao, Impacts of potential models on calculating the thermal conductivity of graphene using non-equilibrium molecular dynamics simulations, *Int J. Heat Mass Transfer* **107**, 450 (2017).
- [46] L. A. Girifalco, M. Hodak, and R. S. Lee, Carbon nanotubes, buckyballs, ropes, and a universal graphitic potential, *Phys. Rev. B* **62**, 13104 (2000).
- [47] C. Y. Chen, Y. She, H. Xiao, J. Ding, J. Cao, and Z. X. Guo, Enhancing the ballistic thermal transport of silicene through smooth interface coupling, *J. Phys.: Condens. Matter* **28**, 145003 (2016).
- [48] P. K. Schelling, S. R. Phillpot, and P. Keblinski, Comparison of atomic-level simulation methods for computing thermal conductivity, *Phys. Rev. B* **65**, 144306 (2002).
- [49] Z. Fan, L. F. C. Pereira, H. Q. Wang, J. C. Zheng, D. Donadio, and A. Harju, Force and heat current formulas for many-body potentials in molecular dynamics simulations with applications to thermal conductivity calculations, *Phys. Rev. B* **92**, 094301 (2015).
- [50] L. T. Kong, Phonon dispersion measured directly from molecular dynamics simulations, *Comput. Phys. Commun.* **182**, 2201 (2011).
- [51] J. Zhang, X. Huang, Y. Yue, J. Wang, and X. Wang, Dynamic response of graphene to thermal impulse, *Phys. Rev. B* **84**, 235416 (2011).
- [52] T. Yamamoto, K. Watanabe, and K. Mii, Empirical-potential study of phonon transport in graphitic ribbons, *Phys. Rev. B* **70**, 245402 (2004).
- [53] S. Ghosh, W. Bao, D. L. Nika, S. Subrina, E. P. Pokatilov, C. N. Lau, and A. A. Balandin, Dimensional crossover of thermal transport in few-layer graphene, *Nat. Mater.* **9**, 555 (2010).
- [54] H. Y. Cao, Z. X. Guo, H. Xiang, and X. G. Gong, Layer and size dependence of thermal conductivity in multilayer graphene nanoribbons, *Phys. Lett. A* **376**, 525 (2012).
- [55] Z. Fan, W. Chen, V. Vierimaa, and A. Harju, Efficient molecular dynamics simulations with many-body potentials on graphics processing units, *Comput. Phys. Commun.* **218**, 10 (2017).
- [56] Z. Fan, L. F. C. Pereira, P. Hirvonen, M. M. Ervasti, K. R. Elder, D. Donadio, T. Ala-Nissila, and A. Harju, Thermal conductivity

- decomposition in two-dimensional materials: Application to graphene, *Phys. Rev. B* **95**, 144309 (2017).
- [57] X. Gu, Y. Wei, X. Yin, B. Li, and R. Yang, *Colloquium: Phononic thermal properties of two-dimensional materials*, *Rev. Mod. Phys.* **90**, 041002 (2018).
- [58] D. L. Nika, E. P. Pokatilov, A. S. Askerov, and A. A. Balandin, Phonon thermal conduction in graphene: Role of Umklapp and edge roughness scattering, *Phys. Rev. B* **79**, 155413 (2009).
- [59] L. Lindsay, D. A. Broido, and N. Mingo, Flexural phonons and thermal transport in graphene, *Phys. Rev. B* **82**, 115427 (2010).
- [60] D. Singh, J. Y. Murthy, and T. S. Fisher, Mechanism of thermal conductivity reduction in few-layer graphene, *J. Appl. Phys.* **110**, 044317 (2011).
- [61] D. L. Nika and A. A. Balandin, Phonons and thermal transport in graphene and graphene-based materials, *Rep. Prog. Phys.* **80**, 036502 (2017).
- [62] Z. X. Guo, D. Zhang, and X. G. Gong, Manipulating thermal conductivity through substrate coupling, *Phys. Rev. B* **84**, 075470 (2011).
- [63] G. Zhang and B. Li, Thermal conductivity of nanotubes revisited: Effects of chirality, isotope impurity, tube length, and temperature, *J. Chem. Phys.* **123**, 114714 (2005).
- [64] H. Shi, Z. Zhan, Z. Qi, K. Huang, E. v. Veen, J. Á. Silva-Guillén, R. Zhang, P. Li, K. Xie, H. Ji, M. I. Katsnelson, S. Yuan, S. Qin, and Z. Zhang, Large-area, periodic, and tunable intrinsic pseudo-magnetic fields in low-angle twisted bilayer graphene, *Nat. Commun.* **11**, 371 (2020).
- [65] M. Koshino and Y. W. Son, Moiré phonons in twisted bilayer graphene, *Phys. Rev. B* **100**, 075416 (2019).
- [66] L. Lindsay, D. A. Broido, and N. Mingo, Flexural phonons and thermal transport in multilayer graphene and graphite, *Phys. Rev. B* **83**, 235428 (2011).
- [67] A. I. Cocemasov, D. L. Nika, and A. A. Balandin, Phonons in twisted bilayer graphene, *Phys. Rev. B* **88**, 035428 (2013).
- [68] X. F. Zhou, Y. W. Liu, C. Y. Hao, C. Yan, Q. Zheng, Y. N. Ren, Y. X. Zhao, K. Watanabe, T. Taniguchi, and L. He, Coexistence of reconstructed and unreconstructed structures in the structural transition regime of twisted bilayer graphene, *Phys. Rev. B* **107**, 125410 (2023).
- [69] The formation of a moiré junction can be owing to the competition between the interlayer vdW coupling and the intralayer elastic deformation, which determines the stacking configurations in TBG. For the TBG with a large twist angle, the size of the moiré pattern is quite small and the structure is energetically preferable. Whereas, for the TBG with a small twist angle, the size of the moiré pattern becomes quite large and the structure becomes less stable. Then, to minimize the total energy of the system, there is a strain-accompanied lattice reconstruction that results in large stacking domains [68]. It is noted that the lattice reconstruction effect would be more remarkable with the decrease of the interlayer distance, due to the enhancement of the interlayer interaction. As a result, when the interlayer distance is reduced to 2.5 Å, the moiré junction is formed in TBGs with small twist angle.
- [70] S. Li, Z. X. Guo, and J. W. Ding, Interface thermal transport of graphene-based intralayer heterostructures, *Physica B (Amsterdam, Neth.)* **561**, 164 (2019).
- [71] A. N. Kolmogorov and V. H. Crespi, Registry-dependent interlayer potential for graphitic systems, *Phys. Rev. B* **71**, 235415 (2005).
- [72] Y. Cheng, Z. Fan, T. Zhang, M. Nomura, S. Volz, G. Zhu, B. Li, and S. Xiong, Magic angle in thermal conductivity of twisted bilayer graphene, *Mater. Today Phys.* **35**, 101093 (2023).